Modelling of Vortex-Induced Loading on a Single-Blade Installation Setup

Skrzypinski, Witold Robert; Gaunaa, Mac; Heinz, Joachim Christian

Published in:
Journal of Physics: Conference Series (Online)

Link to article, DOI:
10.1088/1742-6596/753/8/082037

Publication date:
2016

Document Version
Publisher's PDF, also known as Version of record

Modelling of Vortex-Induced Loading on a Single-Blade Installation Setup

2016 J. Phys.: Conf. Ser. 753 082037

(http://iopscience.iop.org/1742-6596/753/8/082037)

Modelling of Vortex-Induced Loading on a Single-Blade Installation Setup

Witold Skrzypiński, Mac Gaunaa, Joachim Heinz

Department of Wind Energy, Technical University of Denmark (DTU)

wisk@dtu.dk

Abstract. Vortex-induced integral loading fluctuations on a single suspended blade at various inflow angles were modeled in the presents work by means of stochastic modelling methods. The reference time series were obtained by 3D DES CFD computations carried out on the DTU 10MW reference wind turbine blade. In the reference time series, the flapwise force component, *Fx*, showed both higher absolute values and variation than the chordwise force component, *Fz*, for every inflow angle considered. For this reason, the present paper focused on modelling of the *Fx* and not the *Fz* whereas *Fz* would be modelled using exactly the same procedure. The reference time series were significantly different, depending on the inflow angle. This made the modelling of all the time series with a single and relatively simple engineering model challenging. In order to find model parameters, optimizations were carried out, based on the root-mean-square error between the Single-Sided Amplitude Spectra of the reference and modelled time series. In order to model well defined frequency peaks present at certain inflow angles, optimized sine functions were superposed on the stochastically modelled time series. The results showed that the modelling accuracy varied depending on the inflow angle. None the less, the modelled and reference time series showed a satisfactory general agreement in terms of their visual and frequency characteristics. This indicated that the proposed method is suitable to model loading fluctuations on suspended blades.

1. Introduction

Year by year, global electricity consumption grows by about 5%. At the same time, EU countries work on meeting the EU's target for 20% renewable energy in the overall energy supply by 2020. This pushes the wind energy industry to harvest wind at remote offshore sites characterized by relatively high average wind speeds and high wind availability. The Levelized Energy Cost (LEC) of offshore wind farms – being the ratio of all the costs and the energy produced over the farm's lifetime – is significantly influenced by high installation costs. The installation costs include the rental of installation equipment – vessels, cranes and yokes – together with the crews. The problem is that the high average wind speeds, being the reason to install wind turbines at those locations, hamper the installations of wind turbine blades as such installations can only be carried out at relatively low wind speeds. This forces the crews to stand by and wait for weather windows, prolonging the rental and increasing the sites LEC in the end. For a medium size offshore wind farm, the cost of stand-by during the installation averages at about 15 million Euro. This creates a demand to improve the current installation methods by increasing the wind speed threshold for blade installation. In order to do so, accurate aerodynamic and aeroelastic models of single-blade as well as whole-rotor installation setups need to be developed. Gaunaa et al. [1] model the first-order aerodynamic and aeroelastic behavior of a single-blade installation setup subject to turbulent wind of arbitrary direction. The authors compare

the results obtained with their engineering model with the results obtained in the aeroelastic code, HAWC2 [2], achieving a satisfactory agreement. A more constrained setup, namely the Horizontal Single Blade Mounting (HSBM), is analyzed by Kuijken [3] who utilizes a 3D steady-state Reynolds Averaged Navier Stokes (RANS) CFD model in ANSYS Fluent, and an aeroelastic HAWC2 model. Kuijken defines the critical parameters affecting the blade response as well as proposes improvements to the current setup. In terms of the aerodynamic response, a single-blade installation setup has common features with blades at standstill conditions, also referred to as parked blades. The aerodynamic response of those is investigated by Bertagnolio et al. [4], Gaunaa and Larsen [5], Riziotis et al. [6], Zou et al. [7], and Skrzypiński et al. [8,9,10]. The common feature is that the turbulent wind may approach the blade at any direction, including those where deep stall occurs. On the other hand, the aeroelastic responses in both cases are significantly different as a blade during installation is not rigidly clamped and therefore experiences a different modal response. None the less, learning from the state-of-the-art aerodynamic modelling of blades at standstill conditions, one could infer that the modelling of single-blade installations could possibly benefit from the inclusion of some additional unsteady effects, vortex-induced loading [6,7,8] also referred to as static stall [4] among others. An approach to model vortex-induced integral loading fluctuations by means of stochastic modelling methods – previously utilized in wind turbine aerodynamics by Luhur et al. [11] – is described in the current paper. The blade utilized in the present work is the one from the DTU 10MW Reference Wind Turbine by Bak et al. [12]. Fluctuations of the integral loading due to flow separation were modelled in the present work. The engineering model was tuned using the results of present 3D unsteady Detached Eddy Simulation (DES) CFD computations carried out in EllipSys 3D [13,14,15]. The vortex shedding induced forces modelled in the present work are one of the two factors representing the unsteady aerodynamic loading in the standstill or blade installation cases. The other part is the unsteady loading due to turbulent inflow. Being built on the classical crossflow principle, it is described by Gaunaa et al. [1]. Later, Gaunaa et al. [16] investigate the subject deeper, showing that the crossflow principle is, in fact, not the best approach to describe the yawed/tilted cases. Therefore, a new correction model is described in [16]. Such a model may be expanded to create a full-blown engineering model that can predict both the steady and unsteady loading due to constant or turbulent inflow. Combination of such an engineering model, the present one, and specific scaling laws, constitutes tools needed to determine, in an engineering manner, the full aerodynamic loading in the standstill or blade installation cases.

2. Approach and methods

2.1. Description of the CFD solver and mesh generation

EllipSys3D [13,14,15] is an incompressible finite volume CFD solver on a structured grid utilizing curvilinear coordinates. The Detached Eddy Simulations (DES) employed a Reynolds averaged Navier Stokes (RANS) solution in areas close to the blade surface and Large Eddy Simulations (LES) in areas outside the boundary layer where the turbulent length scales became larger than the given grid resolution. The RANS equations were closed with the k-ω SST (Shear Stress Transport) turbulence model by Menter [17]. The DES capabilities were implemented as proposed in Menter and Kuntz [18]. Different inflow conditions were simulated by rotating and inclining the inflow directions relatively to the CFD mesh. The utilized spherical mesh of the DTU 10MW RWT blade [12] exhibited 128 cells in the spanwise direction, 256 cells in the chordwise direction and 192 cells into the normal direction of the blade surface. The height of the first boundary layer cell was set to $2*10^{-6}$ m. Computations were carried out with an inflow velocity of 12 m/s and the time step of 0.0015 s. This resulted in a CFL number of approximately 0.1 in the areas behind the blade where vortex structures needed to be resolved.

2.2. Analysis of the Reference Time Series

Selection of the reference CFD results, obtained in EllipSys3D [13,14,15] described in Section 2.1. , is presented in Figure 1. In the present work, 3 tilt angles were considered initially, i.e. -60°, -30°, 0°. The angle is zero when the flow is perpendicular to the blade, and 90° when the flow is parallel to the blade, from the tip to the root. For each tilt angle, 8 angles of attack (AOA) were considered (40°, 85°, 125°, 165°, 205°, 245°, 295°, 325°), two force components (*Fx* – flapwise, *Fz* - chordwise), each time series 450 second long. It was observed that the force variation for the tilt angle of -60° was very small relative to other tilt angles; therefore its modelling was omitted. The flapwise force component, *Fx*, showed both higher absolute values and variation than the chordwise force component, *Fz*, for every inflow angle considered. For this reason, the present paper focuses on modelling of the *Fx* and not the *Fz* whereas *Fz* would be modelled using exactly the same procedure. Note that the reference time series are very different, depending on the inflow angle. This makes the modelling of all the time series with a single and relatively simple engineering model more challenging.

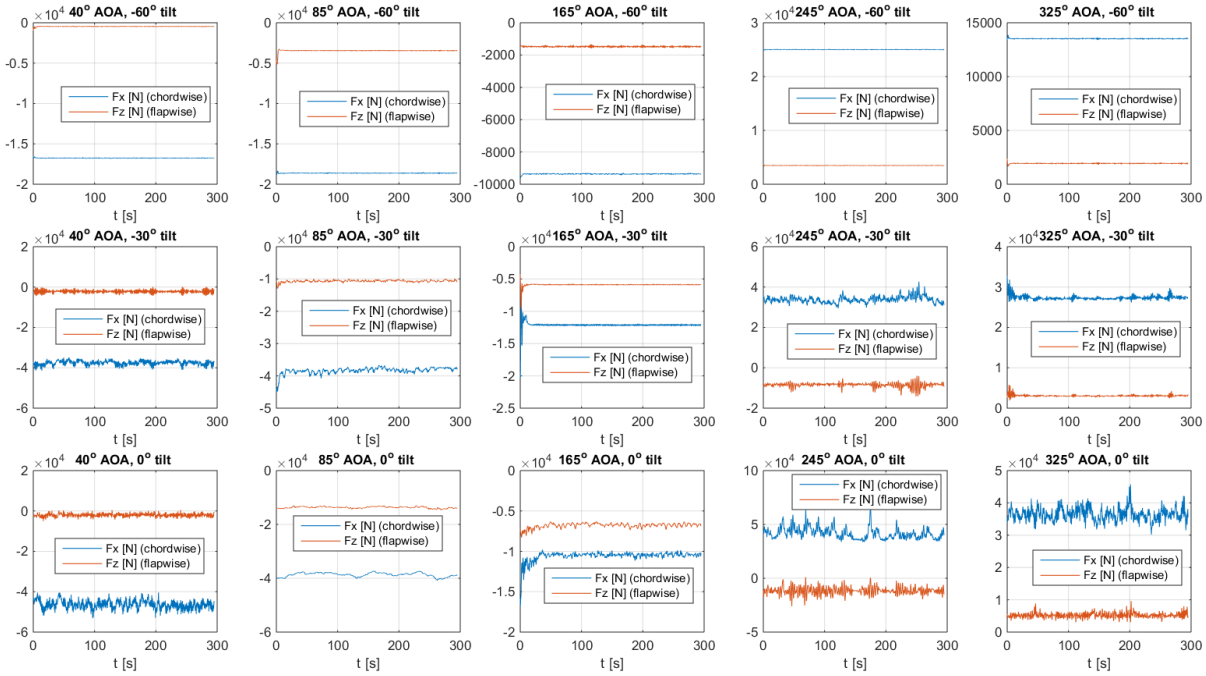

Figure 1: Reference CFD results - integral force components on the blade

2.3. General Description of the Model

The current approach was inspired by that of Luhur et al. [11] where the Langevin process is used to model complex statistics by means of stochastic dynamics. Luhur et al. focus on modelling of the aerodynamic response of an airfoil under turbulent inflow at angles of attack up to 28° where stall and vortex shedding naturally occur. The current work focused on modelling of the response at arbitrary inflow angles including those where deep stall and associated vortex shedding occur. The Langevin equation [11] is a first-order stochastic differential equation based on drift and diffusion functions coupled with a noise term. A thorough study of the definition and handling of different drift and diffusion estimates in Langevin processes is presented by Gottschal and Peinke [19]. For the present application, the Langevin equation in its discrete form looks as follows:

$$X_{i+1}(\alpha, \Psi) = dt\, D^{(1)}(X, \alpha, \Psi) + \sqrt{dt\, D^{(2)}(X, \alpha, \Psi)}\,\Gamma_{i+1} \qquad (1)$$

where $X(t,\alpha,\Psi)$ is an aerodynamic force component, α is the angle of attack at 60 m blade span, Ψ is the tilt angle, and $\Gamma(t)$ is a Gaussian white noise referred to as Langevin force with zero mean value and variance equal to 2. The $D^{(1)}(X,\alpha,\Psi)$ and $D^{(2)}(X,\alpha,\Psi)$ are referred to as the drift and diffusion functions, respectively, also known as the first and second Kramers-Moyal coefficients for $X(t,\alpha,\Psi)$. The $D^{(1)}(X,\alpha,\Psi)$, in general, reflects the deterministic part of the system and estimates the mean change of $X(t,\alpha,\Psi)$ whereas the $D^{(2)}(X,\alpha,\Psi)$ estimates the amplitude of the stochastic fluctuations. Note that the values of those functions depend on the time step, *dt*, and would need to be adjusted if the time step was changed. In the present application, $D^{(1)}(X,\alpha,\Psi)$ was used to assure that the modelled time series would not diverge further from its mean value than the reference did. In practical terms, the amplitude of the reference had been found prior to modelling, and corresponding boundaries were imposed on the model. Therefore, $D^{(1)}$ was predetermined for each inflow angle using the reference and did not undergo an optimization, in contrast to $D^{(2)}$. The shapes of the drift and diffusion functions, presented in Figure 2, were predetermined in the present work based on the analysis of previous work as well as the reference time series. For each inflow angle, those functions preserve their shapes but their exact values change. The exact values of the parameters defining $D^{(2)}$ were found for each inflow angle by means of an optimization. $D^{(2)}$ was the function of the force, of the form ax^2+b. The optimization was based on the root-mean-square error (RMSE) between the Single-Sided Amplitude Spectra (SSAS) of the reference and modelled time series. The modelled time series typically showed more high frequency content than the reference. Similar behaviour is observed in [11]. To mitigate this effect, a low-pass Butterworth filter was applied on the modelled time series. For each inflow angle, the value of the cutoff frequency and the filter order were determined by the optimizer.

Note that although the reference CFD computations were carried out on the DTU 10MW RWT blade, previous work [8] indicates that dimensionless characteristics of vortex-induces aerodynamic phenomena may be relatively insensitive of blade geometry. If this assumption proves right, it will be possible to scale present modelling in order to apply it on blades of various sizes.

Further, note that although the current model is presented in the context of vortex-induced flapwise force variations, it is actually the aerodynamic moments that may have the largest influence on the stability of the single blade installation setup. None the less, the present method is suitable for modelling of vortex-induced variations of the aerodynamic moments as well.

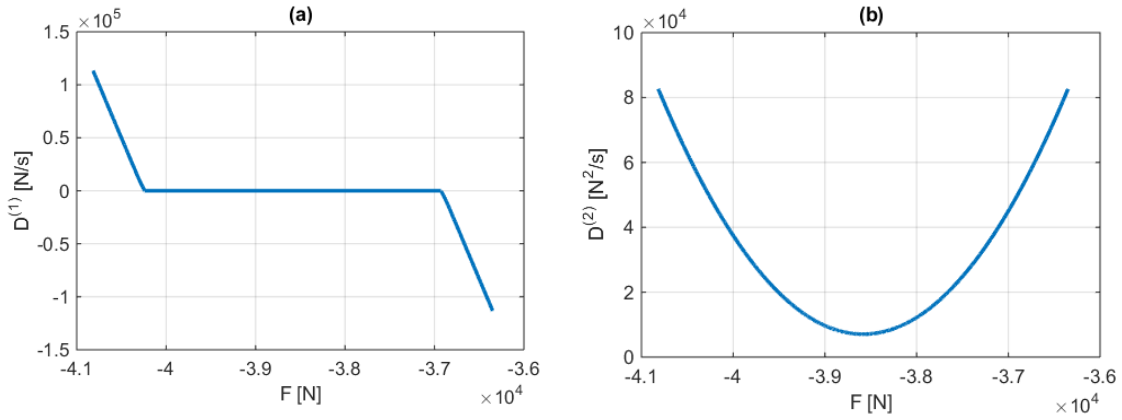

Figure 2 (a): Exemplary drift function, $D^{(1)}$ (b) Exemplary diffusion function, $D^{(2)}$

2.4. Extension of the Model

Analysis of the reference time series showed a difference between forces obtained at inflow approximately perpendicular to the blade and at other inflow angles. This difference is depicted in Figure 3. Figure 3(a) presents a comparison of the time series obtained at 40° and 85° AOA, respectively. Both time series were obtained at 0° tilt. Figure 3(b) presents Single-Sided Amplitude

Spectra of the corresponding time series. It is visible in Figure 3(b) that the SSAS of the time series obtained at 85° AOA does not show any peaks. This may easily be modelled with the method presented in Section 2.3. On the other hand, the time series corresponding to 40° AOA may be approximated by a straight line in a loglog graph only outside the frequency range of 0.4-3 Hz. In this range, several frequency peaks are present with the dominant at 0.7 Hz with the amplitude of approximately 1kN. The corresponding amplitudes were marked in Figure 3(a). Such oscillations were accounted for by the superposition of a sine function on the modelled time series. The frequency and amplitude of the sine function were determined from the reference time series and did not undergo optimization. It is recommended that at least the dominating frequency peak is represented. None the less, depending of the desired fidelity, one may choose to represent several frequency peaks, if present. In the present work, a maximum of one sine function was used for each time series.

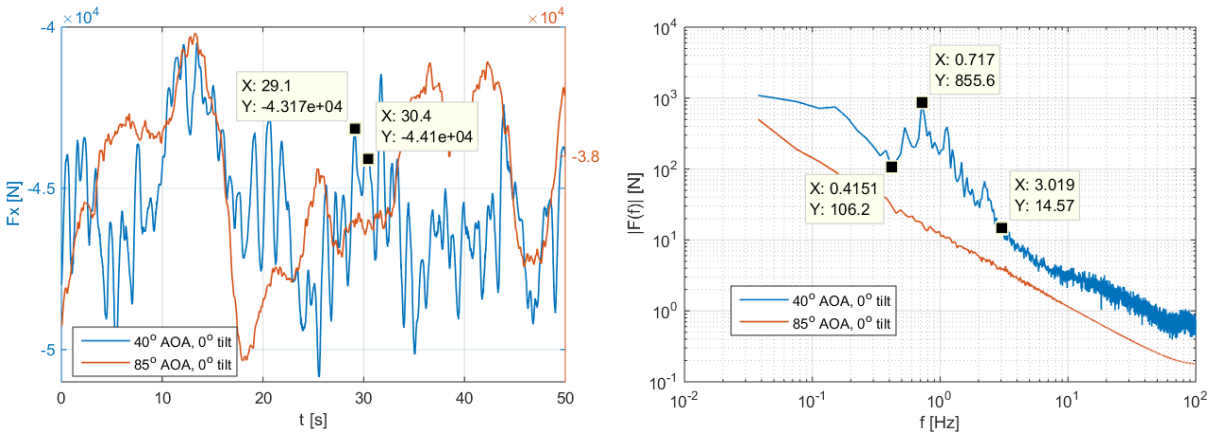

Figure 3: (a) Zoomed-in reference time series at 40° and 85° AOA, respectively (b) Single-Sided Amplitude Spectra of the same time series

3. Description of the results

Figure 4 and Figure 5 present the reference CFD time series and the time series modelled using the method described in the previous sections, together with their Single-Sided Amplitude Spectra.

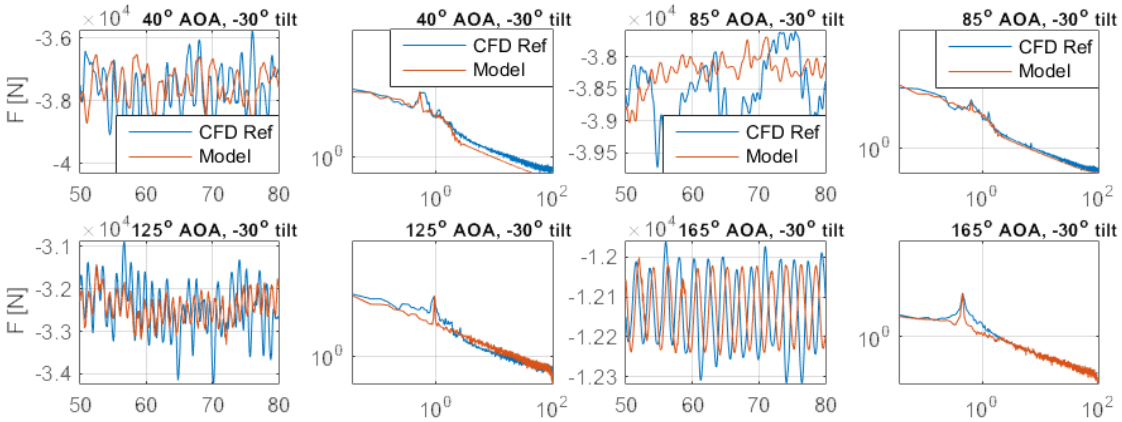

Figure 4: (1st and 3rd column) CFD reference and modelled time series; (2nd and 4th column) Single-Sided Amplitude Spectra of the corresponding time series

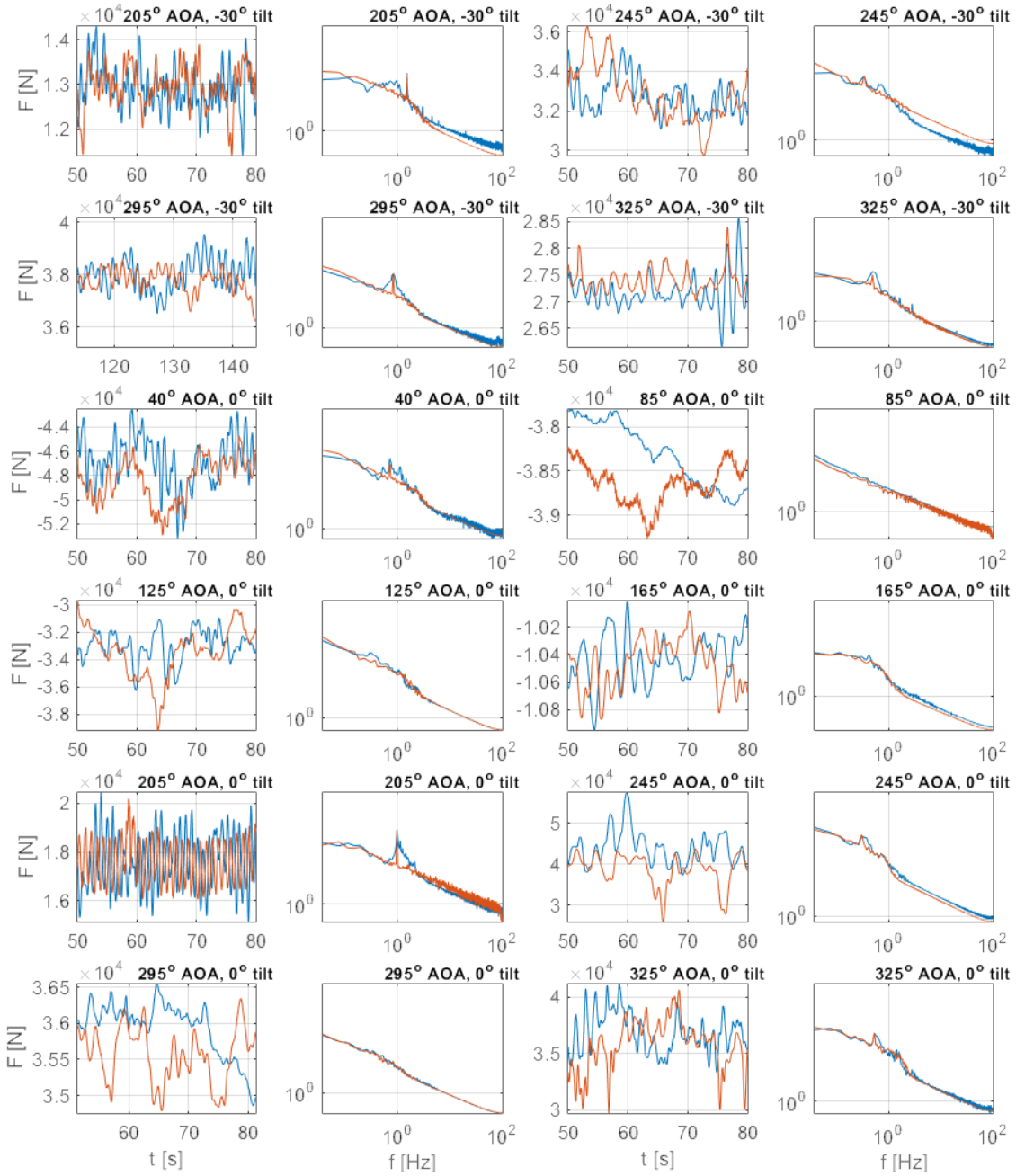

Figure 5: (1st and 3rd column) CFD reference and modelled time series; (2nd and 4th column) Single-Sided Amplitude Spectra of the corresponding time series

The results show that the modelling accuracy varies depending on the inflow angle. None the less, the modelled and reference time series show a satisfactory general agreement in terms of their visual and frequency characteristics.

Note that in the current work effort was made to balance the accuracy and robustness of the model. In other words, the model was intended for variety of inflow angles where the corresponding time series are very different. This compromise needs to be met in order to easily model the aerodynamic characteristics of suspended blades subject to random inflow angles.

Figure 6(a) presents the amplitudes, A, and Figure 6(b) presents the frequencies, f, of the deterministic part of the modelled time series. Note that the amplitudes at 0° tilt show more variability

with respect to the AOA than the amplitudes at -30° tilt. The reason for that might be that at 0° tilt, a certain change in the AOA corresponds to a higher change in the overall inflow angle than at -30° tilt. In order to understand that, one may consider the extreme case of -90° tilt where the flow is parallel to the blade and it is at all impossible to vary the AOA. The frequency values presented in Figure 6(b) are generally higher for the -30° tilt than for the 0° tilt. This may be associated with the higher spanwise flow correlation at -30° tilt but this should be looked into in more detail if future work. Figure 6(c) and Figure 6(d) present the two parameters defining the quadratic equation for $D^{(2)}$, i.e. a and b in the ax^2+b type equation, respectively.

One of the characteristics of the parameter a presented in Figure 6(c) is the shape similarity between the -30° and 0° tilt curves. This feature is less pronounced for the parameter b presented in Figure 6(d). The last two parameters determined by the optimization were the cutoff frequency and order of the low-pass Butterworth filter, presented in Figure 7.

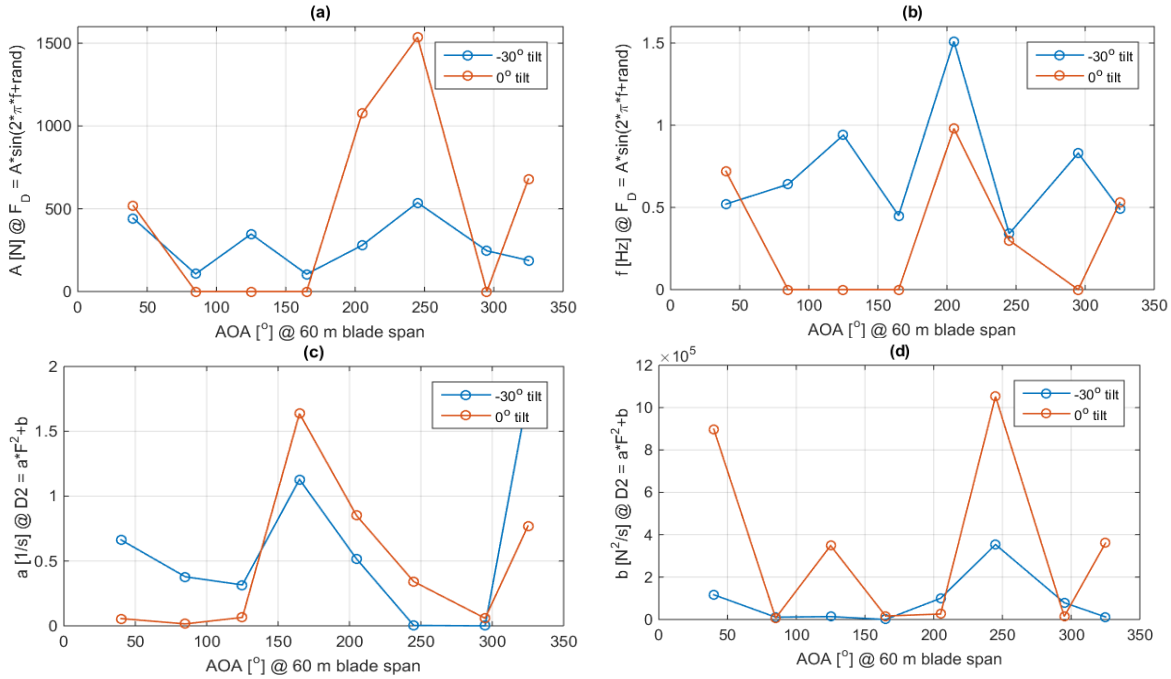

Figure 6: (a,b) The parameters of the sine fuction determining the deterministic part of the modelled time series (c,d) The parameters determining the shape of the $D^{(2)}$; all plotted as a function of the AOA at 60 m blade span, and for the -30° and 0 ° tilt angles

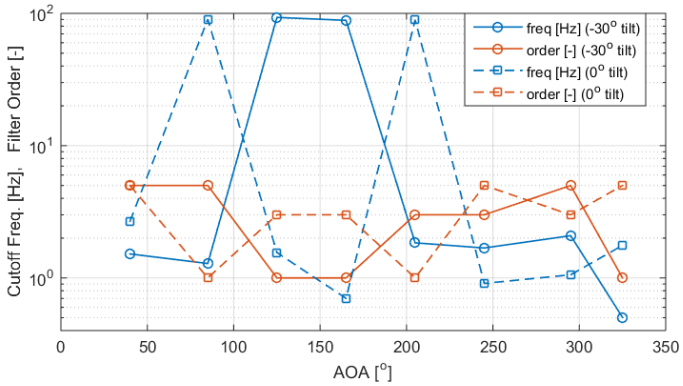

Figure 7: The cutoff frequency and corresponding order of the low-pass Butterworth filter applied on the modelled time series, as a function of the AOA at 60 m blade span.

One of the characteristic features of the presented curves is that when the optimizer chose a relatively high cutoff frequency of 100 Hz, at the same it chose a low filter order of 1. Mind that the lower the filter order is, the weaker the effect of the filter is. This indicates that at those specific angles, the filter was, in practical terms, unnecessary. Generally, the reference time series showed very much difference between different inflow angles. This was reflected in most of the parameters governing the modelled time series as those parameters typically significantly varied from one inflow angle to another.

4. Conclusions

Vortex-induced integral loading fluctuations on a single suspended blade at various inflow angles were modeled in the presents work. This was carried out by means of stochastic modelling methods – previously utilized in wind turbine aerodynamics by Luhur et al. [20]. The reference time series were obtained by 3D DES CFD computations carried out on the DTU 10MW reference wind turbine blade [12]. In the reference time series, the flapwise force component, *Fx*, showed both higher absolute values and variation than the chordwise force component, *Fz*, for every inflow angle considered. For this reason, the present paper focused on modelling of the *Fx* and not the *Fz* whereas *Fz* would be modelled using exactly the same procedure.

The reference time series were very different, depending on the inflow angle which made the modelling of all the time series with a single and relatively simple engineering model challenging.

In order to find model parameters, optimizations were carried out, based on the root-mean-square error between the Single-Sided Amplitude Spectra of the reference and modelled time series.

In order to model well defined frequency peaks present at certain inflow angles, predetermined sine functions were superposed on the stochastically modelled time series resulting from the optimizations.

The results showed that the modelling accuracy varied depending on the inflow angle. None the less, the modelled and reference time series showed a satisfactory general agreement in terms of their visual and frequency characteristics. This indicated that the proposed method is suitable to model loading fluctuations on suspended blades.

The vortex shedding induced forces modelled in the present work are one of the two factors representing the unsteady aerodynamic loading in the standstill or blade installation cases. The other part is the unsteady loading due to turbulent inflow, described by Gaunaa et al. [16]. Combination of such an engineering model, the present one, and specific scaling laws, constitutes tools needed to determine, in an engineering manner, the full aerodynamic loading in the standstill or blade installation cases.

5. Future work

The present work focused on modelling of vortex-induced variation of a single component of integral force on a suspended blade. Before full-blown engineering model may be applied on various suspended blades at various conditions, at least three aspects concerning the present method need to be addressed in future work, on top of combining the present model with the one described by Gaunaa et al. [16]:

- Investigate the extent to which different blades share the same aerodynamic characteristics at high AOA's.
- Choose an efficient method of including the correlation between modelled force components.
- Scale the modelled forces, moments and time step depending on the modelled wind speed and blade length relative to the respective reference values.

A natural continuation of the present work would be to adjust and implement a deep-stall engineering model in an aeroelastic code. That would be carried out with the scope on modelling blade vibrations at standstill conditions together with other load cases where deep stall occurs. In order to do so, several aspects would need to be addressed:

- The model would need to be applied on sectional and not integral level.
- The relation between spanwise vortex-induced load correlation and blade oscillation would need to be established and taken into account in the model.
- The phenomenon of lock-in would need to be investigated in the present context and accounted for in the model.

References

[1] Gaunaa, M., Bergami, L., Guntur, S., & Zahle, F. (2014). First-order aerodynamic and aeroelastic behavior of a single-blade installation setup. Journal of Physics: Conference Series (Online), 524, [012073]. 10.1088/1742-6596/524/1/012073

[2] Larsen, T.J. (2009). How 2 HAWC2 the user's manual Tech. Rep. R-1597(EN) Risoe National Laboratory. Technical University of Denmark

[3] Kuijken, L. (2015) Single Blade Installation for Large Wind Turbines in Extreme Wind Conditions, Master of Science Thesis, Technical University of Denmark & TU Delft

[4] Bertagnolio, F., Rasmussen, F., Sørensen, N.N., Johansen, J., Madsen H.A. (2010) A stochastic model for the simulation of wind turbine blades in stochastic stall. Wind Energy 2010; 13: 323–338

[5] Gaunaa, M., Larsen, T.J. (2002) Stilstandslaster. In Forskning i Aeroelasticitet. Bak C (ed.). Risø DTU National Laboratory for Sustainable Energy: Roskilde, Denmark, 2002, Risø-R-1434(DA) in Danish.

[6] Riziotis, V.A., Voutsinas, S.G., Politis, E.S., Chaviaropoulos, P.K. (2010) Stability analysis of parked wind turbine blades using a vortex model. Proceedings of TORQUE 2010: The Science of Making Torque from Wind, Crete, Greece, 28–30 June, 2010.

[7] Zou, F., Riziotis, V. A., Voutsinas, S. G., and Wang, J. (2015) Analysis of vortex-induced and stall-induced vibrations at standstill conditions using a free wake aerodynamic code. Wind Energ., 18: 2145–2169. doi: 10.1002/we.1811.

[8] Skrzypiński, W. R., Gaunaa, M., Sørensen, N. N., Zahle, F., & Heinz, J. C. (2014). Vortex-induced vibrations of a DU96-W-180 airfoil at 90° angle of attack. Wind Energy, 17(10), 1495-1514. 10.1002/we.1647

[9] Skrzypiński, W. R., Gaunaa, M., Sørensen, N. N., Zahle, F., & Heinz, J. C. (2014). Self-induced vibrations of a DU96-W-180 airfoil in stall. Wind Energy, 17(4), 641-655. 10.1002/we.1596

[10] Skrzypiński, W. R., & Gaunaa, M. (2015). Wind turbine blade vibration at standstill conditions — the effect of imposing lag on the aerodynamic response of an elastically mounted airfoil. Wind Energy, 18(3), 515–527. 10.1002/we.1712

[11] Luhur, M. R., Peinke, J., Schneemann, J. and Wächter, M. (2015). Stochastic modeling of lift and drag dynamics under turbulent wind inflow conditions, Wind Energ., 18, pages 317–337, doi: 10.1002/we.1699

[12] Bak, C., Zahle, F., Bitsche, R., Kim, T., Yde, A., Henriksen, L. C., ... Natarajan, A. (2013). The DTU 10-MW Reference Wind Turbine [Sound/Visual production (digital)]. Danish Wind Power Research 2013, Fredericia, Denmark, 27/05/2013

[13] Michelsen, JA. (1992). Basic3D—a platform for development of multiblock PDE solvers. Report AFM 92-05, Dept. of Fluid Mechanics, Technical University of Denmark, DTU, Denmark, 1992

[14] Michelsen, JA. (1994). Block structured multigrid solution of 2D and 3D elliptic PDE's. Report AFM 94-06, Dept. of Fluid Mechanics, Technical University of Denmark, DTU, Denmark, 1994.

[15] Sørensen, NN. (1995). General purpose flow solver applied to flow over hills. PHD Dissertation, Risø-R-827(EN), Risø National Laboratory, Roskilde, Denmark, 1995.

[16] Gaunaa, M., Heinz, J. C., Skrzypiński, W. (2016). Aerodynamic Forces Acting on Wind Turbine Blades in Quasisteady Standstill and Blade Installation Situations. Extended Abstract submitted for the Torque 2016 conference.
[17] Menter, FR. (1994). Two-equation eddy-viscosity turbulence models for engineering applications, AIAA Journal, Vol. 32, No. 8, pp. 1598-1605
[18] Menter, FR., Kuntz, M. (2004). Adaptation of Eddy-Viscosity Turbulence Models to Unsteady Separated Flow Behind Vehicles. In R. McCallen, F. Browand, & J. Ross (Eds.), The Aerodynamics of Heavy Vehicles: Trucks, Buses, and Trains (pp. 339–352). Berlin, Heidelberg: Springer Berlin Heidelberg. doi:10.1007/978-3-540-44419-0_30
[19] Gottschal, J., Peinke, J. (2008). On the definition and handling of different drift and diffusion estimates, New Journal of Physics 10 (2008) 083034 (20pp), 10.1088/1367-2630/10/8/083034
[20] Luhur, M. R., Peinke, J., Schneemann, J. and Wächter, M. (2015). Stochastic modeling of lift and drag dynamics under turbulent wind inflow conditions, Wind Energ., 18, pages 317–337, doi: 10.1002/we.1699